A benchmark study of a capacitively coupled oxygen discharge of the oopd1 particle-in-cell Monte Carlo code

2013 Plasma Sources Sci. Technol. 22 035011

(http://iopscience.iop.org/0963-0252/22/3/035011)

Plasma Sources Sci. Technol. **22** (2013) 035011 (11pp) doi:10.1088/0963-0252/22/3/035011

A benchmark study of a capacitively coupled oxygen discharge of the oopd1 particle-in-cell Monte Carlo code

J T Gudmundsson[1,2,4], **E Kawamura**[3] **and M A Lieberman**[3]

[1] University of Michigan–Shanghai Jiao Tong University Joint Institute, Shanghai Jiao Tong University, 800 Dong Chuan Road, Shanghai 200240, People's Republic of China
[2] Science Institute, University of Iceland, Dunhaga 3, IS-107 Reykjavik, Iceland
[3] Department of Electrical Engineering and Computer Sciences, University of California, Berkeley, CA 94720, USA

E-mail: tumi@hi.is

Received 4 January 2013, in final form 4 April 2013
Published 20 May 2013
Online at stacks.iop.org/PSST/22/035011

Abstract
The oopd1 particle-in-cell Monte Carlo collision (PIC-MCC) code is used to simulate a capacitively coupled discharge in oxygen. oopd1 is a one-dimensional object-oriented PIC-MC code in which the model system has one spatial dimension and three velocity components. It contains a model for planar geometry and will contain models for cylindrical and spherical geometries, and replaces the xpdx1 series, which is not object-oriented. The oopd1 also allows for different weights of simulation particles and relativistic treatment of electrons. The revised oxygen model includes, in addition to electrons, the oxygen molecule in the ground state, the oxygen atom in the ground state, the negative ion O^- and the positive ions O^+ and O_2^+. The cross sections for the collisions among the oxygen species have been significantly revised from earlier work using the xpdp1 code and the electron kinematics have been enhanced. Here we make a benchmark study and compare the oopd1 code to the well-established planar xpdp1 code and discuss the differences using a limited cross section set with O_2^+ ions, O^- ions and electrons as the charged particles. We compare the electron energy distribution function, the electron temperature profile, the density profiles of charged particles and electron heating rates for a capacitively coupled oxygen discharge at 50 mTorr with electrode separation of 4.5 cm. Then we explore the effect of adding O atoms and O^+ ions on the overall discharge.

(Some figures may appear in colour only in the online journal)

1. Introduction

The particle-in-cell Monte Carlo (PIC-MC) method is a self-consistent kinetic approach capable of predicting the electron energy distribution function (EEDF) and ion energy distribution function (IEDF) for ions arriving at substrates. The basic idea of PIC simulation is to allow thousands of computer-simulated particles (superparticles) to represent many more (10^{14}–10^{18} m^{-3}) real particles. In a PIC simulation the motion of each particle is simulated and macro-quantities (such as particle density, particle flux, current density etc) are calculated from the position and velocity of these particles [1, 2]. The macro-force acting on the particles is calculated from the field equations. The object-oriented plasma device one (oopd1) code [3] is a one-dimensional object-oriented PIC code [4]. In 1d-3v PIC codes, such as oopd1, the model system has one spatial dimension and three velocity components. oopd1 contains a model for planar geometry and will contain models for cylindrical and spherical geometries, and thus replaces the xpdx1 series [5], which is not object-oriented. A one-dimensional description of the system is sufficient when modeling a capacitively coupled discharge due to the large ratio of transverse to longitudinal dimensions.

The oxygen discharge is of vital importance in various material processing applications such as ashing of photoresist,

[4] Author to whom any correspondence should be addressed.

etching of polymer films and oxidation and deposition of thin film oxides. The oxygen chemistry is rather involved, in particular due to the presence of metastable molecular and atomic oxygen and detachment processes. The oxygen chemistry has been explored using global (volume averaged) models [6–10]. These studies indicate that at low pressures ($\leqslant$10 mTorr) and in particular at higher absorbed power the discharge is highly dissociated, oxygen atoms can dominate the discharge and the O^+-ion can be the dominant charged particle [6, 7]. Furthermore, electron-impact detachment and ion–ion neutralization dominate the loss of negative ions at low pressures, while detachment by oxygen atoms dominates at higher pressures ($\geqslant$20 mTorr). The contribution of detachment by the metastable molecule $O_2(a\,^1\Delta_g)$ is much smaller and highest, roughly 20%, at 100 mTorr.

The Monte Carlo collision (MCC) model for the oxygen discharge was described by Vahedi and Surendra [11] and applied to explore the density profiles of charged particles in an oxygen discharge which was also compared with theoretical prediction [12]. One-dimensional (1D) PIC-MCC simulations of various configurations of oxygen and Ar/O_2 discharges, both symmetrical and asymmetrical, over a range of pressures using the xpdx1 series have been compared with experimental findings, showing good agreement [13]. Babaeva *et al* [14] explored the formation of the IEDF in an O_2/Ar mixture in an asymmetric capacitively coupled discharge using a 1D cylindrical model (xpdc1). Roberto *et al* [15] used the xpdp1 code to investigate the influence of the secondary electron emission on the density profiles and the EEDF. Other 1D PIC-MCC codes have been developed to explore the oxygen discharge. Bronold *et al* [16] applied a 1D PIC-MCC model, which includes the metastable oxygen molecule $O_2(a\,^1\Delta_g)$, to a capacitively coupled rf discharge in oxygen and used it to determine the IEDF [17]. Schüngel *et al* [18] used a 1D PIC-MCC code to explore the electrical asymmetry effect in a capacitively coupled oxygen discharge. Bera *et al* [19, 20] used a PIC-MCC hybrid model to explore the low-pressure capacitively coupled rf discharge, in particular the electron power absorption and the influence of pressure on the energetics and particle densities. In all of these works only electrons, the positive ion O_2^+, and the negative ion O^- are treated kinetically and the positive ion O^+ is neglected. Here we add O atoms and O^+ ions to the discharge model for oxygen, including reactions for electron-impact ionization and excitation of the oxygen atom, charge exchange with the oxygen atom and molecule and mutual neutralization with the negative ion O^-. The purpose of this work is to introduce the new oopd1 code, describe its features and benchmark it against the well-established xpdp1 code. The oopd1, like the xpdp1 code, is a general plasma device simulation tool capable of simulating various types of plasmas, including processing discharges, accelerators and beams, and breakdown. Thus relativistic treatment of electrons has been implemented. Particle weight is the number of real particles each superparticle represents, i.e. the ratio of the number of physical particles to computational particles. In oopd1 the particles can have different weights. As the neutral gas density is much higher than the densities of charged species, different weights allow us to treat both charged particles and neutral particles kinetically. In this work we discuss the revised reaction set in section 2. We briefly describe the difference between xpdp1 and oopd1 in section 3 and then compare the simulation results using the oopd1 code and the xpdp1 code using both the revised cross section set and revised electron kinematics in section 4. Then we demonstrate the oopd1 code using the complete revised reaction set including O atoms and O^+ ions in section 5.

2. The oxygen reaction set

The cross sections for the collisions among the oxygen species have been significantly revised from the earlier work of Vahedi and Surendra [11], used in the xpdx1 series. The reaction set for oxygen is shown in table 1. The reactions included in xpdp1 are marked by x. The cross section used for elastic scattering of electrons off of the oxygen molecule is the one recommended by Itikawa [21]. The cross section for the metastable excitation $O_2(A\,^3\Sigma_u^+, A'\,^3\Delta_u, c\,^1\Sigma_u^-)$ is taken from Shyn and Sweeney [22] and Green *et al* [23] as recommended by Itikawa [21]. Other cross sections for electron-impact excitation and dissociation of the oxygen molecule are the same as used by Vahedi and Surendra [11] and originate from Phelps *et al* [24, 25]. The dissociation of the oxygen molecule is treated as an excitation of the oxygen molecule, which subsequently breaks into fragments. The electron transition is assumed to be rapid on a nuclear timescale. The excitation to the 6.12 eV level leads to dissociation into $O(^3P) + O(^3P)$, excitation to the 8.4 eV level leads to dissociation into $O(^3P) + O(^1D)$, and excitation to the 9.97 eV level leads to dissociation into $O(^1D) + O(^1D)$, and the released energy to each pair of heavy fragments is 1.03 eV, 1.27 eV and 0.88 eV, respectively. The cross section for electron-impact ionization of the oxygen molecule was measured by Krishnakumar and Srivastava [26] and the ionization potential is 12.06 V. The cross sections for electron scattering, electron-impact ionization and electron-impact excitation to the metastable states $O_2(A\,^3\Sigma_u^+, A'\,^3\Delta_u, c\,^1\Sigma_u^-)$ and the electron-impact excitation to the dissociative levels of the oxygen molecule are shown in figure 1. The rotational, vibrational and electronic excitations are included to serve as an additional energy loss mechanism for electrons. Rotational excitation has been found to be relatively unimportant while vibrational excitations are found to considerably influence the shape of the EEDF [11]. The cross sections for electron-impact excitation of the rotational and vibrational states and electron-impact excitation to the metastable $a\,^1\Delta_g$ and $b\,^1\Sigma_g^+$ states of the oxygen molecule are shown in figure 2. For the dissociative attachment from the ground state oxygen molecule, the cross section is taken from Rapp and Briglia [27]. The threshold energy is 4.2 eV and the incident electron loses its energy which is absorbed by the oxygen molecule to form O_2^- which subsequently dissociates to form the fragments O and O^-. The electron transition is assumed to be rapid on a nuclear timescale, and the energy of the ejected fragments can be calculated applying the Frank–Condon principle. The potential energy for the $O + O^-$ pair is 3.63 eV above the ground state potential for O_2. The remaining incident electron

Table 1. The reaction set for oxygen used in the oopd1 code.

Reaction	Process	In xpdp1	Reference
Electron-impact O_2			
$e + O_2 \longrightarrow O_2 + e$	Elastic scattering	x	[21]
$e + O_2(r = 0) \longrightarrow e + O_2(r > 0)$	Rotational excitation	x	[25]
$e + O_2(v = 0) \longrightarrow e + O_2(v > 0)$	Vibrational excitation	x	[25]
$e + O_2 \longrightarrow e + O_2(a\,^1\Delta_g)$	Metastable excitation (0.98 V)	x	[25]
$e + O_2 \longrightarrow e + O_2(b\,^1\Sigma_g^+)$	Metastable excitation (1.63 V)	x	[25]
$e + O_2 \longrightarrow e + O_2(A\,^3\Sigma_u^+, A'\,^3\Delta_u, c\,^1\Sigma_u^-)$	Metastable excitation (4.05 V)	x	[21–23]
$e + O_2 \longrightarrow O(^3P) + O(^3P) + e$	Dissociation (6.12 V)	x	[25]
$e + O_2 \longrightarrow O(^3P) + O(^1D) + e$	Dissociation (8.4 V)	x	[25]
$e + O_2 \longrightarrow O(^1D) + O(^1D) + e$	Dissociation (9.97 V)	x	[25]
$e + O_2 \longrightarrow O_2^+ + 2e$	Electron-impact ionization (12.06 V)	x	[26]
$e + O_2 \longrightarrow e + O + O(3p^3P)$	Dissociative excitation (14.7 V)	x	[25]
$e + O_2 \longrightarrow O + O^-$	Dissociative attachment	x	[27]
$e + O_2 \longrightarrow O^+ + O^- + e$	Polar dissociation		[27]
$e + O_2 \longrightarrow O^+ + O + 2e$	Dissociative ionization		[26]
Electron-impact O			
$e + O \longrightarrow O + e$	Elastic scattering		[29, 30]
$e + O(^3P) \longrightarrow O(^1D) + e$	Excitation to ^1D (1.96 eV)		[31]
$e + O(^3P) \longrightarrow O(^1S) + e$	Excitation to ^1S (4.18 eV)		[31]
$e + O(^3P) \longrightarrow O(^3P^0) + e$	Excitation to $^3P^0$ (15.65 eV)		[31]
$e + O(^3P) \longrightarrow O(^5S^0) + e$	Excitation to $^5S^0$ (9.14 eV)		[31]
$e + O(^3P) \longrightarrow O(^3S^0) + e$	Excitation to $^3S^0$ (9.51 eV)		[31]
$e + O \longrightarrow O^+ + 2e$	Ionization (13.62 eV)		[32]
Detachment			
$e + O^- \longrightarrow O + 2e$	Electron-impact detachment	x	[39]
$O^- + O_2 \longrightarrow O + O_2 + e$	Detachment by oxygen molecule	x	[40]
$O^- + O \longrightarrow O_2 + e$	Detachment by oxygen atom		[41]
Recombination			
$e + O_2^+ \longrightarrow O(^3P) + O(^1D)$	Dissociative recombination	x	[33, 34]
$O^- + O_2^+ \longrightarrow O + O_2$	Mutual neutralization	x	[37, 36]
$O^+ + O^- \longrightarrow O + O$	Mutual neutralization		[37, 38]
Charge exchange			
$O_2^+ + O_2 \longrightarrow O_2 + O_2^+$	Charge exchange	x	[42–44]
$O^+ + O_2 \longrightarrow O + O_2^+$	Charge exchange		[46]
$O^+ + O \longrightarrow O + O^+$	Charge exchange		[47]
$O_2^+ + O \longrightarrow O_2 + O^+$	Charge exchange (1.56 eV)		[48, 51]
$O_2^+ + O_2 \longrightarrow O^+ + O + O_2$	Fragmentation by energetic O_2^+		See text
Scattering			
$O^- + O_2 \longrightarrow O^- + O_2$	Scattering	x	[49]
$O + O_2 \longrightarrow O + O_2$	Scattering	x	[45]
$O_2^+ + O_2 \longrightarrow O_2^+ + O_2$	Scattering	x	See text
$O^+ + O_2 \longrightarrow O^+ + O_2$	Scattering		See text
$O_2 + O_2 \longrightarrow O_2 + O_2$	Scattering		[45]
$O + O \longrightarrow O + O$	Scattering		See text

energy ($\mathcal{E}_{inc} - 3.63$ eV) is divided between the fragments. The cross section for dissociative ionization is taken from the measurement of Krishnakumar and Srivastava [26]. The ionization potential for dissociative ionization is 18.73 V [28]. The cross section for polar dissociation is taken from the measurements of Rapp and Briglia [27]. The cross sections for electron-impact polar dissociation, dissociative attachment and dissociative ionization of the oxygen molecule are shown in figure 3. To include O^+ ions a number of reactions had to be added. The cross section for elastic collisions of electrons with oxygen atoms is assembled from the theoretical calculations by Thomas and Nesbet [29] for $E < 2$ eV and from the review by Itikawa and Ichimura [30] for $E > 2$ eV. The cross sections for electron-impact excitation of atomic oxygen to the ^1D, ^1S, $^3P^0$, $^5S^0$ and $^3S^0$ states are taken from the review by Laher and Gilmore [31]. The cross section for electron-impact ionization is taken from the theoretical work of Kim and Desclaux [32]. The ionization potential is 13.62 V. The cross sections for elastic scattering off the oxygen atom and electron-impact excitation and ionization of the oxygen atom are shown in figure 4.

The cross section for dissociative recombination

$$e + O_2^+ \longrightarrow O(^3P) + O(^1D)$$

is taken by combining the measurement data of Mul and McGowan [33] and Peverall *et al* [34]. Dissociative recombination is assumed to create $O(^3P)$ and $O(^1D)$ in equal amounts [35]. The cross section for mutual neutralization of O^- and O_2^+ is taken from a measurement by Padgett and Peart [36] and combined with the measurement of Olson [37] which we scale down by a factor of 5 to fit the more recent work.

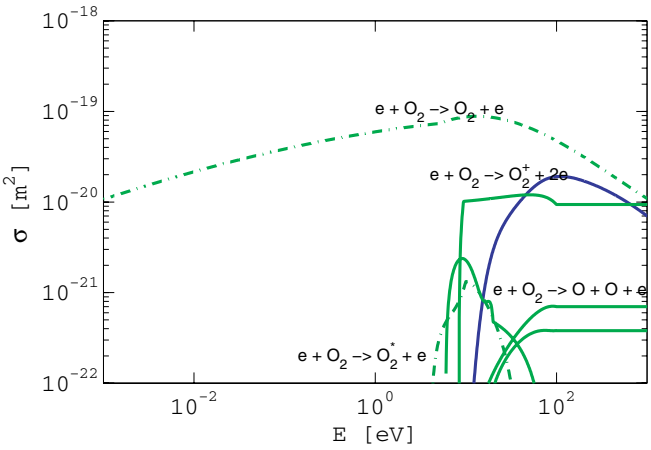

Figure 1. Cross sections for electron scattering, electron-impact ionization and electron-impact excitation to the metastable states $O_2(A\,^3\Sigma_u^+, A'\,^3\Delta_u, c\,^1\Sigma_u^-)$ and the dissociative levels of the oxygen molecule.

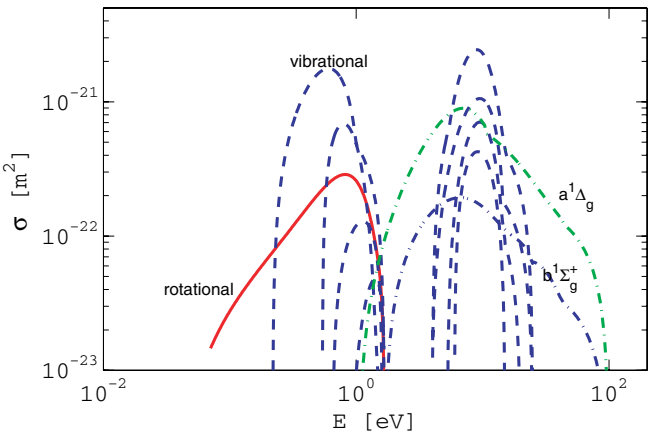

Figure 2. Cross sections for electron-impact excitation of the rotational and vibrational states and to the metastable $a\,^1\Delta_g$ and $b\,^1\Sigma_g^+$ states of the oxygen molecule.

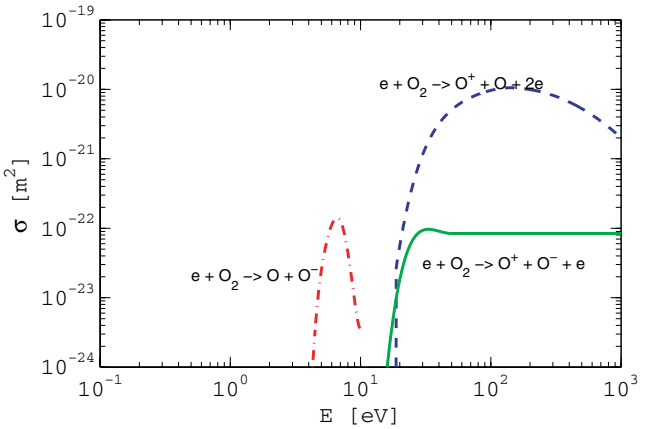

Figure 3. Cross sections for electron-impact polar dissociation, dissociative attachment and dissociative ionization of the oxygen molecule.

Similarly the cross section for mutual neutralization of O^- and O^+ is taken from a measurement by Olson [37] and scaled down by a factor of 6.4 to fit the more recent measurements of Hayton and Peart [38]. The cross sections for mutual neutralization and dissociative recombination are shown in figure 5.

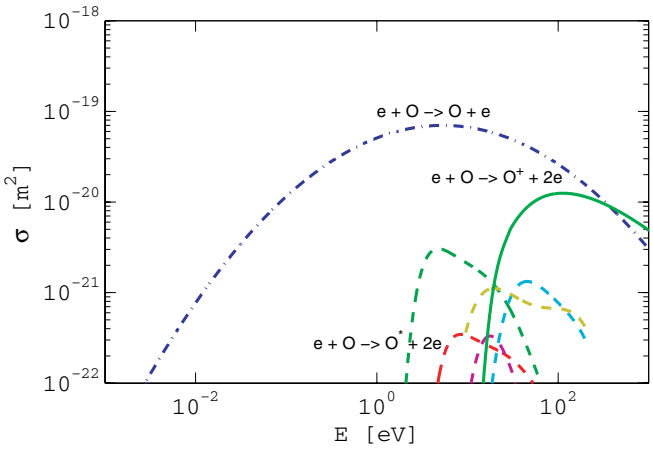

Figure 4. Cross sections for elastic scattering off the oxygen atom and electron-impact excitation and ionization of the oxygen atom.

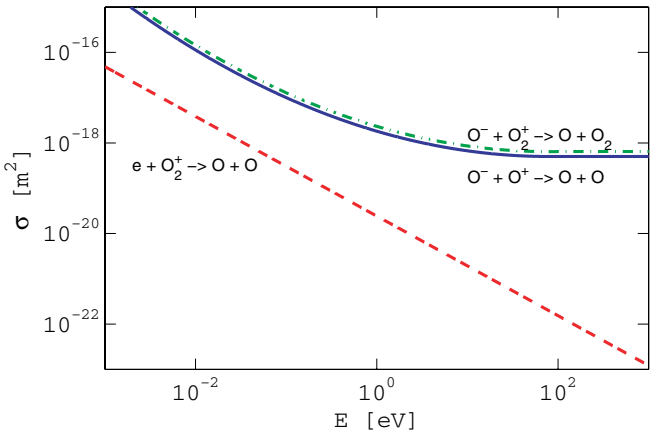

Figure 5. Cross sections for mutual neutralization (at the center of mass (CM) frame) and dissociative recombination.

The cross section for electron-impact detachment is taken from a measurement by Vejby-Christensen *et al* [39]. The threshold energy is 1.46 eV. The cross section for the detachment from the negative oxygen ion by the oxygen molecule was measured by Comer and Schulz [40]. The cross section for detachment by the oxygen atom is calculated from the rate coefficient measured at room temperature by Belostotsky *et al* [41] and it is allowed to scale with $1/\sqrt{\mathcal{E}}$ for ion energy below 184 meV. Above 184 meV the cross section is set to a constant value of 1.09×10^{-19} m^2. The cross sections for detachment by electrons, oxygen atoms and oxygen molecules are shown in figure 6.

For the charge exchange

$$O_2^+ + O_2 \longrightarrow O + O_2^+$$

the cross section is assembled from the cross section given by Ellis *et al* [42] for the energy range 25.9–350 meV, measured by Baer *et al* [43] for the energy range 1–40 eV and measured by Wilcox and Moran [44] for the energy range 0.8–3 keV. The cross section for the elastic scattering of O_2^+ off O_2 is assumed to be half the cross section for charge exchange. The cross section for the scattering of the oxygen atom by the oxygen molecule is taken from Brunetti *et al* [45]. For the charge

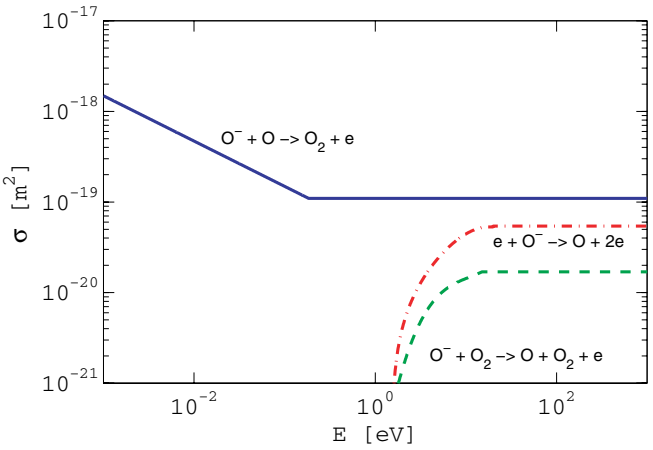

Figure 6. Cross sections for detachment by electrons, oxygen atoms and oxygen molecule (at the CM frame).

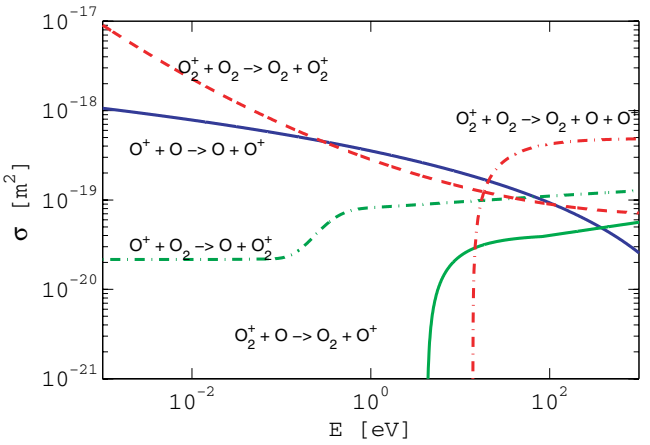

Figure 7. Cross sections for charge exchange and fragmentation involving positive ions. In all cases the cross section is shown in the rest frame of the target (the neutral) versus the energy of the ion as the projectile.

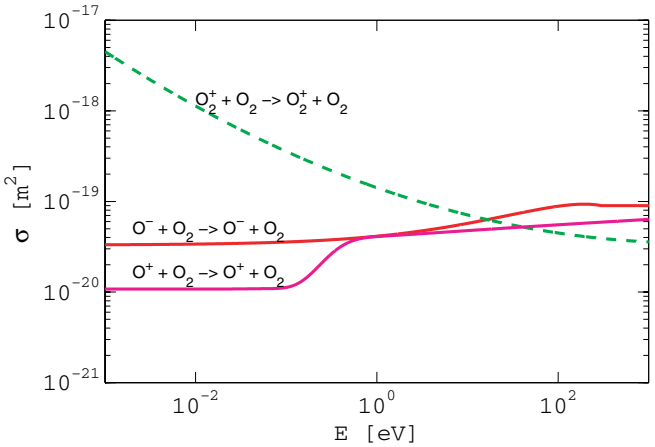

Figure 8. Cross sections for scattering among the heavy charged particles. In all cases the cross section is shown in the rest frame of the target (the neutral) versus the energy of the ion as the projectile.

exchange

$$O^+ + O_2 \longrightarrow O + O_2^+$$

the cross section is taken from a fit given by Lindsay and Stebbings [46]. The cross section for the elastic scattering of O^+ off O_2 is assumed to be half the cross section for charge exchange. For the cross section for the charge exchange

$$O^+ + O \longrightarrow O + O^+$$

a fit given by Stebbings *et al* [47] is used. The cross section for the charge exchange

$$O_2^+ + O \longrightarrow O_2 + O^+$$

was measured by Stebbings *et al* [48]. This cross section was measured in the energy range 80–6000 eV but we extrapolate the data using the form

$$\sigma = \sigma_0 \left(1 - \frac{\mathcal{E}_{\mathrm{Thr}}}{\mathcal{E}}\right) \tag{1}$$

and assume the process has a threshold energy of 1.56 eV. For the elastic scattering of the negative ion O^- off O_2 the cross section is taken from the measurements of Muschlitz [49]. The charge transfer of O^- on O_2 has a threshold energy of ∼1.0 eV, which is much higher than the thermal energy of heavy particles; hence this process is considered unimportant, and neglected. High energy O_2^+ ions can collide with oxygen molecules and fragment into O^+, O, and O_2 or

$$O_2^+ + O_2 \longrightarrow O_2 + O^+ + O$$

where we assume a cross section given by equation (1) where $\sigma_0 = 4.9 \times 10^{-19}$ m^2 is the gas kinetic cross section for O_2 [50, p 312]. The potential energy required to form the $O^+ + O$ pair is 6.9 eV and we assume this process to have threshold energy that is twice this value, or 13.8 eV. The remaining energy difference is split between the fragments. The cross sections for charge exchange and fragmentation by energetic molecular ions are shown in figure 7 and the cross sections for scattering of heavy particles are shown in figure 8. The cross section for scattering of O_2 molecules by O_2 molecules is taken from Brunetti *et al* [45] and extrapolated to high and lower energy assuming a constant cross section. Scattering of O atoms by O atoms is assumed to be half of the cross section for scattering of O atoms by O_2 molecules measured by Brunetti *et al* [45].

3. The simulation

For the simulation we assume that the plasma is sustained between two parallel plates. One of the electrodes is driven by a voltage source

$$V(t) = V_0 \sin(\omega t), \tag{2}$$

where V_0 is the voltage amplitude. For the benchmark study we assume the discharge to be operated at a single frequency of 13.56 MHz at 50 mTorr and $V_0 = 222$ V with an electrode separation of 4.5 cm. We assume a large capacitor of 1 F in series with the voltage source. These are the same parameters as explored in Lichtenberg *et al* [12] using the xpdp1 code

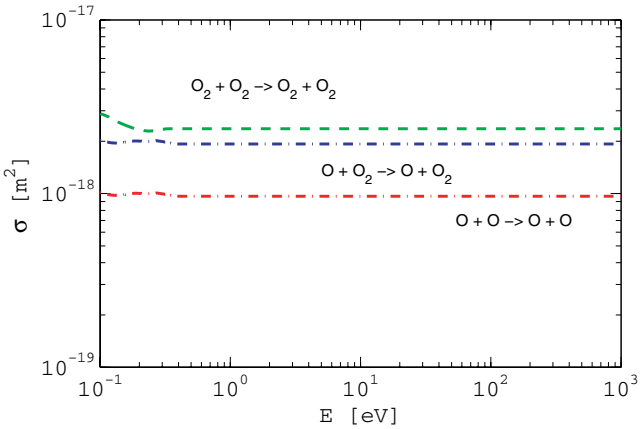

Figure 9. Cross sections for scattering among the heavy neutral particles.

except there the discharge was driven by 0.4 A rf current source. In this work we neglect secondary electron emission. As the neutral gas density is much higher than the densities of charged species, the neutral gas was treated as a background with fixed density and temperature. Here it is assumed that the oxygen gas (the neutral gas species O and O_2) is maintained uniformly in space, i.e. the neutral particles are not followed as particles unless their energy exceeds a preset threshold value. However, in some electron–neutral collisions, the target neutral particles gain some energy or leave the collision in an excited state. But the most common electron–neutral collision will be between electrons and the background low temperature gas particles if the population of the energetic and/or excited neutrals is low. The neutral background species are assumed to have a Maxwellian velocity distribution at the gas temperature (e.g. $T_n = 26\,\text{mV}$). We choose a sub-cycling factor of 16 for the heavy particles and assume parabolic initial density profiles [52].

The time step Δt and the grid spacing Δx are chosen to resolve the electron plasma frequency accurately and the electron Debye length of the low-energy electrons or

$$\omega_{pe}\Delta t < 0.2 \tag{3}$$

where ω_{pe} is the electron plasma frequency. The simulation grid is uniform and consists of 1000 cells. The electron time step is chosen to be 3.68×10^{-11} s. The simulation was run for 11×10^6 time steps or 5500 rf cycles.

There are some differences between xpdp1 and oopd1. Particle weight is the number of real particles each superparticle represents, i.e. the ratio of the number of physical particles to computational particles. In xpdp1 all the simulated particles have the same weight; in oopd1 the particles can have different weights [53, 54]. The collisions of particles with different weights were implemented in oopd1 [53] following the method suggested by Miller and Combi [55]. Another difference is that oopd1 and xpdp1 use different algorithms for the scattering of the incident and ejected electrons. In particular xpdp1 uses a non-relativistic algorithm for electron scattering and electron-impact excitation and ionization [11] while oopd1 uses a relativistic algorithm [54]. Furthermore, xpdp1 does not transform electron collisions into the rest frame of the neutral. A relativistic collision model was developed and implemented into the 2D object-oriented xoopic code [56]. These were later implemented to the oopd1 code with improved kinematic calculations and more accurate differential cross sections for calculation of scattering angles and ionization secondary electron energy [54]. For the non-relativistic case xpdp1 uses the non-isotropic differential cross section as described by Vahedi and Surendra [11] and Surendra *et al* [57] while the oopd1 uses the revised differential cross sections for electron scattering given by Okhrimovskyy *et al* [58] where the electron scattering angle χ is found from

$$\cos\chi = 1 - \frac{2R}{1 + 8\epsilon(1 - R)}, \tag{4}$$

where $\epsilon = \mathcal{E}_{inc}/\mathcal{E}_0$, $\mathcal{E}_{inc}$ is the energy of the electron before the collision, $\mathcal{E}_0$ is the atomic unit of energy ($\mathcal{E}_0 = 27.21\,\text{eV}$), and R is a random number uniformly distributed in the interval [0,1].

In oopd1 the velocity and scattering angle are calculated by a relativistic algorithm. However, even though the relativistic kinetic energy equation is valid for the entire energy range, it is more computationally intensive than the classical approximation. Therefore, a criterion is used to determine if relativistic calculations are needed, i.e. if $\frac{1}{2}m_e v_e^2 > (\gamma - 1)m_e c^2$, where m_e is the electron mass, $\gamma = (1 - \beta^2)^{-1/2}$ is the Lorentz factor, $\beta = v_e/c$ and v_e is the velocity of the incoming electron, and c is the speed of light. The relativistic collision model modifies the velocity and scattering angle of the charged particles after a collision [54]. This applies to collisions between charged particles and neutral background gas, in particular the electron–neutral collisions: elastic scattering, electron-impact ionization and electron-impact excitation, but not for ion–neutral collisions. For calculation of the scattering angle, the Monte Carlo method is used with a relativistic differential cross section as the distribution function. For relativistic elastic collisions the Wentzel model is used to find the energy of the scattered electron and the scattering angle [54, 59, 60]. Then the differential cross section is obtained from the first Born approximation as

$$\frac{d\sigma(\chi)}{d\Omega} = \frac{(ZZ'e^2)^2}{(p\beta c)^2}\frac{1}{(2A + 1 - \cos\chi)^2} \tag{5}$$

for elastic scattering of particles with charge $Z'e$ by atoms of atomic number Z where p is the momentum and the angular distribution function is

$$f(\chi) = \frac{1}{\pi}\frac{A(1 + A)}{(2A + 1 - \cos\chi)^2} \tag{6}$$

and the Molière screening parameter A is given as

$$A = \frac{1}{4}\left(\frac{h}{p}\right)^2 (0.885Z^{-1/3}a_0)^{-2}(1.13 + 3.76(\alpha Z/\beta)^2) \tag{7}$$

where h is Planck's constant, p is the momentum, a_0 is the Bohr radius, Z is the atomic number of the target, and $\alpha = 1/137$

is the fine-structure constant. The cumulative distribution function gives the scattering angle

$$\cos\chi = 2A + 1 + \frac{2A(A+1)}{R - A - 1}. \tag{8}$$

Note that the scattering angle given by equation (8) is with respect to the direction of incident electron and thus we need to transform it into the laboratory frame, using a geometric coordinate transformation.

Excitation is treated like elastic collision with a reduced energy. It is assumed that the incident particle transfers energy to the neutral atom in order excite it, so the energy loss of the incident particles is equal to the excitation threshold and the energy of the scattered electron is

$$\mathcal{E}_{\rm scat} = \mathcal{E}_{\rm inc} - \mathcal{E}_{\rm ex}, \tag{9}$$

where $\mathcal{E}_{\rm inc}$ is the energy of the incident electron, and $\mathcal{E}_{\rm ex}$ is the excitation threshold. For electron-impact ionization collisions an electron–ion pair is created and the energy balance becomes

$$\mathcal{E}_{\rm scat} + \mathcal{E}_{\rm ej} + \mathcal{E}_{\rm i} = \mathcal{E}_{\rm inc} + \mathcal{E}_{\rm N} - \mathcal{E}_{\rm iz}, \tag{10}$$

where $\mathcal{E}_{\rm ej}$ is the energy of the ejected electron, $\mathcal{E}_{\rm iz}$ is the ionization threshold, $\mathcal{E}_{\rm N}$ is the energy of the target neutral atom and $\mathcal{E}_{\rm i}$ is the energy of the created ion. Due to the large ion-to-electron mass ratio, we can assume that the momentum of the incident electron is much less than the momentum of the neutral atoms. So the incident electron strips an electron off the neutral, and the neutral becomes an ion, continuing on its trajectory virtually undisturbed and

$$\mathcal{E}_{\rm i} = \mathcal{E}_{\rm N}. \tag{11}$$

This assumption allows us to rewrite the above energy balance equation as

$$\mathcal{E}_{\rm scat} + \mathcal{E}_{\rm ej} = \mathcal{E}_{\rm inc} + \mathcal{E}_{\rm iz}. \tag{12}$$

To find the energy of the ejected electron $\mathcal{E}_{\rm ej}$ we use the differential ionization cross section $\sigma(\mathcal{E}_{\rm inc}, \mathcal{E}_{\rm ej}, \mathcal{E}_{\rm iz})$ and write

$$R = \frac{\int_0^{\mathcal{E}_{\rm ej}} \sigma(\mathcal{E}_{\rm inc}, \mathcal{E}_{\rm ej}, \mathcal{E}_{\rm iz})\, {\rm d}\mathcal{E}_{\rm ej}}{\int_0^{\frac{\mathcal{E}_{\rm ej}-\mathcal{E}_{\rm iz}}{2}} \sigma(\mathcal{E}_{\rm inc}, \mathcal{E}_{\rm ej}, \mathcal{E}_{\rm iz})\, {\rm d}\mathcal{E}_{\rm ej}}, \tag{13}$$

where R is a random number [0,1]. This equation is solved for $\mathcal{E}_{\rm ej}$ by inverting the distribution function. Since the ionization threshold energy and the incident electron energy are known and the ejected electron energy is calculated from equation (13), equation (12) gives the scattered electron energy. Once the scattered electron energy is found the scattering angle of incident electron and that for the created electron is calculated in a manner similar to that of an elastic collision. However, obtaining the scattering angle requires a doubly differential cross section for relativistic collisions [54]. It should be noted that the relativistic treatment has negligible effect in typical processing plasmas as discussed here.

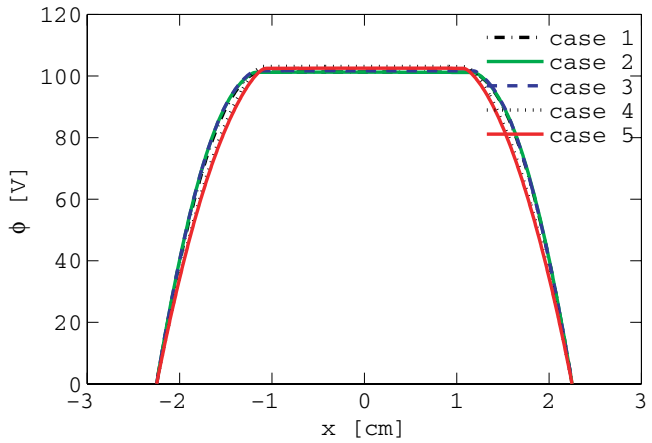

Figure 10. Potential profile for a parallel plate capacitively coupled oxygen discharge at 50 mTorr with a gap separation of 4.5 cm by a 222 V voltage source at 13.56 MHz.

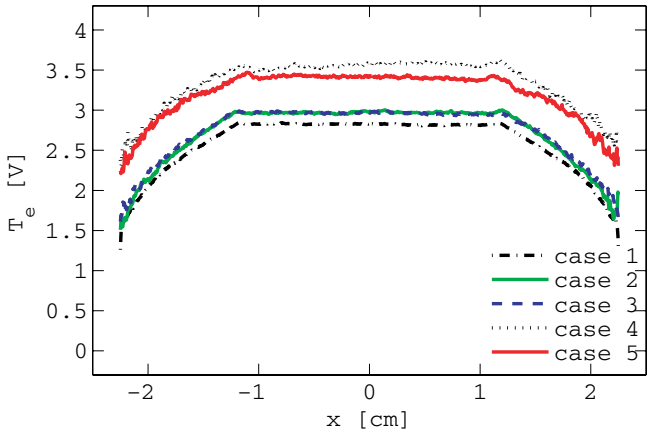

Figure 11. Electron temperature profile for a parallel plate capacitively coupled oxygen discharge at 50 mTorr with a gap separation of 4.5 cm by a 222 V voltage source at 13.56 MHz.

4. Comparison of xpdp1 and oopd1

To benchmark the code we first compare the first four cases listed in table 2. Case 1 uses the xpdp1 code with the xpdp1 cross section set and fully non-relativistic electron scattering algorithm as described by Vahedi and Surendra [11]. Case 2 uses the oopd1 code but with the xpdp1 cross section set and non-relativistic electron scattering algorithm as described by Vahedi and Surendra [11]. Case 3 uses the oopd1 code with the xpdp1 cross section set and the revised algorithm for electron scattering as well as relativistic treatment if needed as described by Lim [54]. Case 4 is using the oopd1 code but with the revised cross section set, but including only the reactions that were included in xpdp1, marked with an x in table 1 and the revised algorithm for electron scattering as well as relativistic treatment for electron scattering, if needed. Note that for these four cases only O_2^+ ions, O^- ions and electrons are followed as charged particles. In all cases the particle weight, i.e. the ratio of the number of physical particles to computational particles, is set to be 10^7 for all particles.

The potential profile for the four cases explored is shown in figure 10. The potential profile is almost the same for

Table 2. The cases explored and numerical values of selected plasma parameters at the center of the discharge.

Case	Code	Cross section set	Electron kinematics	ϕ_0	n_{e0} (m^{-3})	n_- (m^{-3})	n_+ (m^{-3})	T_{eff0} (V)	α_0
1	xpdp1	xpdp1	xpdp1	101.30	2.43×10^{14}	1.17×10^{16}	1.20×10^{16}	2.83	48.3
2	oopd1	xpdp1	xpdp1	101.25	2.29×10^{14}	1.21×10^{16}	1.23×10^{16}	2.98	52.8
3	oopd1	xpdp1	oopd1	101.75	2.18×10^{14}	1.19×10^{16}	1.20×10^{16}	2.98	54.5
4	oopd1	oopd1 limited	oopd1	103.11	1.55×10^{14}	1.75×10^{16}	1.78×10^{16}	3.59	113.2
5	oopd1	oopd1 full	oopd1	102.55	1.65×10^{14}	1.70×10^{16}	1.71×10^{16}	3.43	102.9

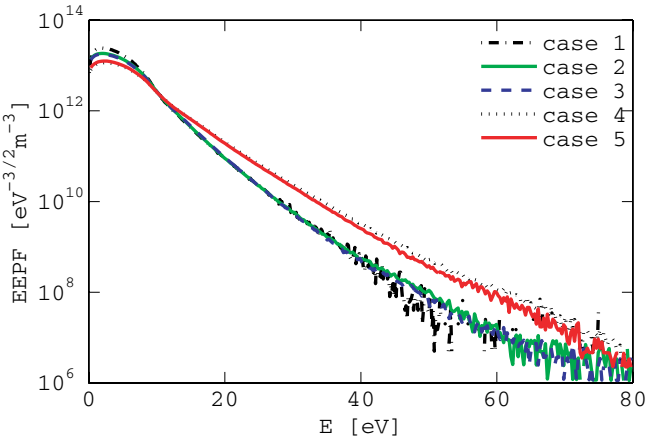

Figure 12. EEPF at the center of a parallel plate capacitively coupled oxygen discharge at 50 mTorr with a gap separation of 4.5 cm by a 222 V voltage source at 13.56 MHz.

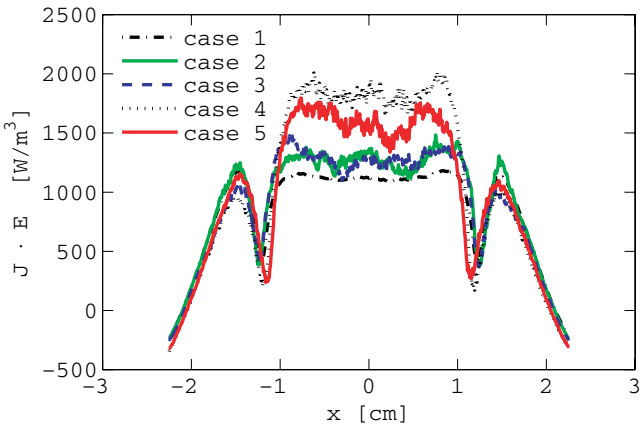

Figure 13. Electron heating rate for a parallel plate capacitively coupled oxygen discharge at 50 mTorr with a gap separation of 4.5 cm by a 222 V voltage source at 13.56 MHz.

case 1, case 2 and case 3, that is for both xpdp1 and oopd1 using the xpdp1 cross sections for both the relativistic and non-relativistic kinematics. When the limited revised cross section set is used, case 4, the potential profile becomes slightly narrower and the center potential increases slightly. Figure 11 shows the effective electron temperature profile for the four cases explored. The effective electron temperature is lower when using xpdp1 than using oopd1 with the xpdp1 cross sections. The effective electron temperature at the center of the discharge is 2.83 V for case 1 and 2.98 V for cases 2 and 3. The center effective electron temperature increases to 3.59 V when using the revised cross section set as seen with case 4. Table 2 also shows numerical values of selected plasma parameters at the center of the discharge. Figure 12 shows the electron energy probability function (EEPF). The EEPF is almost the same for case 1, case 2 and case 3, that is for both xpdp1 and oopd1 using the xpdp1 cross sections for both the relativistic and non-relativistic kinematics. There is a slightly higher density of low-energy electrons when the xpdp1 code is used (case 1) than when the oopd1 code is used. This may explain the slightly lower effective electron temperature observed when using xpdp1 and seen in figure 11. In addition to the differences between xpdp1 and oopdp1 discussed in section 3, xpdp1 uses the electron velocity rather than the relative velocity between incident and target particles for the electron–neutral collisions. Also xpdp1 smoothes the particle densities by passing them through a one-two-one filter [61]. This is carried out to reduce numerical heating by getting rid of high wave-vector components. This has not been implemented in oopd1. This can explain some of the differences between cases 1 and 2. There is an increase in the density of high-energy electrons and slightly lower density of low-energy electrons when the revised cross section set is used in the simulation (case 4).

There are two main heating mechanisms in capacitively coupled discharges: ohmic heating due to electron–neutral collisions and stochastic heating at the plasma edge due to momentum transfer from the moving sheaths. The electron heating rate profile is shown in figure 13. The peaks in the electron heating rates near the plasma–sheath boundaries are mainly due to stochastic heating while the electron heating in the bulk is primarily due to ohmic heating of slow electrons in the bulk plasma. As seen in figure 13, the enhanced treatment of the collision kinematics in oopd1 leads to an increase in the ohmic heating and decrease in the stochastic heating. The revised cross section set further increases the ohmic heating in the bulk plasma and decreases the stochastic heating.

Figure 14 shows the density profiles for O^- ions, O_2^+ ions and electrons for the four cases explored here. The negative ion profile seen in figure 14(*a*) is almost the same for case 1, case 2 and case 3, that is for both xpdp1 and oopd1 using the xpdp1 cross sections. When the limited revised cross section set is used, case 4, the negative ion density profile becomes slightly narrower and the peak density at the discharge center is higher. The same applies to the positive ion density seen in figure 14(*b*). The peak positive ion density is 1.2×10^{16} m^{-3} for cases 1, 2 and 3, that is for oopd1 using the xpdp1 cross sections regardless of the electron kinematics. The revised cross section set gives higher positive ion density at the center of the discharge or 1.8×10^{16} m^{-3}, for case 4. The electron density profile is almost the same for case 1, case 2 and case 3

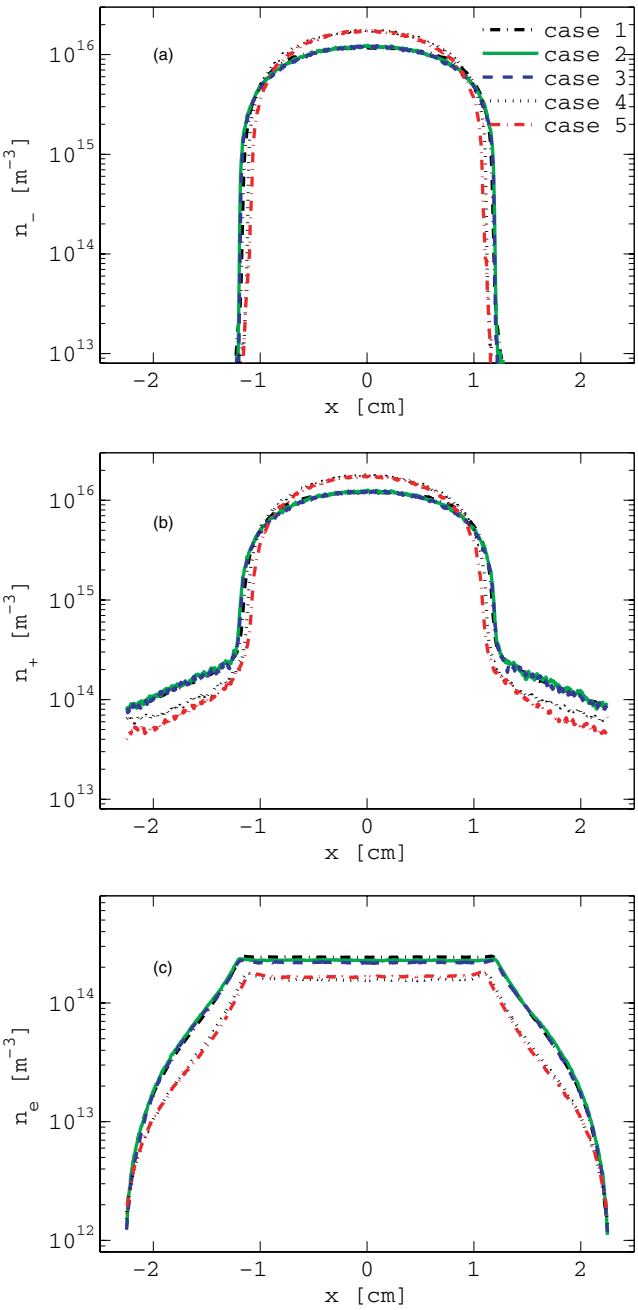

Figure 14. (*a*) O^- ion density profile, (*b*) O_2^+ ion density profile and (*c*) electron density profile for a parallel plate capacitively coupled oxygen discharge at 50 mTorr with a gap separation of 4.5 cm by a 222 V voltage source at 13.56 MHz.

while for case 4 it is narrower and the center density is lower for the revised cross section set. The center electron density is 2.4×10^{14} m^{-3} for case 1, and 2.3×10^{14} m^{-3} for case 2. With the revised reaction set the center electron density drops slightly to 1.6×10^{14} m^{-3} and the profile becomes narrower. Thus here are some differences especially in the effective electron temperature, O_2^+-ion, O^--ion, and electron densities, due to the different reaction dynamics and cross sections used. For example the center electronegativity α_0 increases from about 48 to about 113 when the new cross sections and reaction kinematics are used.

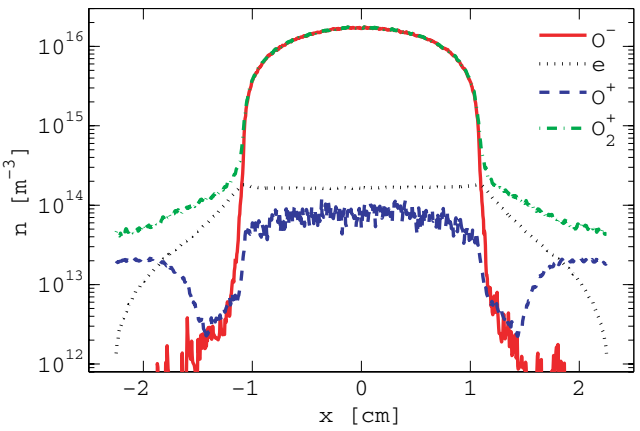

Figure 15. Density profiles for a parallel plate capacitively coupled oxygen discharge at 50 mTorr with a gap separation of 4.5 cm by a 222 V voltage source at 13.56 MHz simulated using the full reaction set (case 5).

5. The influence of O atoms

In case 5 we use a full reaction set for oxygen as listed in table 1. We assume that the electrodes are circular, each having a diameter of 14.36 cm. The power absorbed in the discharge is 1 W and this power is used in the global model to calculate the density ratio of neutral O_2 molecules and and O atoms in the discharge [62]. For the given dimensions, discharge pressure and absorbed power the global model calculations give a partial pressure due to O atoms of 0.087%. So for case 5 we assume 99.913% of the initial background gas is due to O_2 molecules and 0.087% is due to O atoms. The dynamics of the charged particles (electrons, O_2^+, O^+ and O^- ions) was followed as well as the O atoms when their energy exceeds 100 meV. In all cases the particle weight for the charged particles is set to be 10^7 and for the high energy O atoms it is 10^9. This corresponds to about 8 electrons and roughly 420 O_2^+ and O^- ions per cell. As the O atom hits the electrode it returns as a thermal O atom with a 50% probability, or two O atoms can return as a thermal O_2 with a 50% probability. The profile of O atoms with energy above 100 meV is relatively flat at roughly 6×10^{14} m^{-3}. The secondary electron emission yield is assumed to be zero for both O^+ and O_2^+ ions hitting the electrode. Figure 15 shows the density profiles for the charged particles when simulating the capacitively coupled oxygen discharge at 50 mTorr and electrode separation of 4.5 cm using the full reaction set listed in table 1. The density profiles for O^- ions, O_2^+ ions and electrons are almost the same as shown in figures 14(*a*)–(*c*), respectively, for case 4. The electronegativity at the discharge center is 102.9 for case 5 compared with 113.2 for case 4. Note that the oxygen atom density is roughly 1.4×10^{18} m^{-3} so for the given condition the presence of oxygen atoms and O^+ ions does not have much influence on the overall discharge. The density of O atoms with energy exceeding 100 mV is about 1.5×10^{17} m^{-3}. So for these conditions the use of the simplified oxygen reaction set used in many studies [11, 12] is fully justified. The electron heating rate for a parallel plate capacitively coupled oxygen discharge using the full reaction set is also shown in

figure 13. When the oxygen atom is present the ohmic heating in the bulk plasma decreases slightly and the stochastic heating increases slightly compared with neglecting oxygen atoms and O^+ ions. This is also seen in the effective electron temperature profile seen in figure 11. There is a slight decrease in the electron temperature when oxygen atoms are included in the simulation. This decrease in electron temperature is due to a slight decrease in the density of high-energy electrons as seen by comparing the EEPF at the center of the discharge for cases 4 and 5.

6. Conclusion

We demonstrated a newly developed 1d-3v PIC-MCC code oopd1 for simulations of capacitively coupled rf discharges in oxygen. The code includes significantly revised cross section database for collisional processes in oxygen, as well as the addition of O atoms and O^+ ions and the relevant reactions and cross sections. The oopd1 also uses a relativistic algorithm to calculate the electron kinematics in electron scattering, and electron-impact excitation and ionization. We benchmarked the planar model of the oopd1 code against the well-established xpdp1 code. The difference between the two codes is almost entirely due to the revised cross section set used. The addition of O atoms and O^+ ions can have a significant influence on the overall discharge. However, for the case studied here, due to the low density of O atoms, the influence is negligible. Detachment by O atoms and the metastable $O_2(a\,^1\Delta_g)$ molecule is known to be an important loss channel for negative ions in oxygen discharges and has significant influence on electronegativity and the electron heating process. Future work will incorporate the metastable $O_2(a\,^1\Delta_g)$ molecule and its contribution to ionization and detachment.

Acknowledgments

This work was partially supported by the Icelandic Research Fund Grant No 130029-051, by the Department of Energy Office of Fusion Energy Science Contract DE-SC000193, and by the California Industries under University of California Discovery Grant ele07-10283 under the IMPACT program. Discussions with professors J P Verboncoeur and A J Lichtenberg are gratefully acknowledged.

References

[1] Verboncoeur J P 2005 *Plasma Phys. Control. Fusion* **47** A231
[2] Tskhakaya D, Matyash K, Schneider R and Taccogna F 2007 *Contrib. Plasma Phys.* **47** 563
[3] Hammel J and Verboncoeur J P 2003 *Bull. Am. Phys. Soc.* **48** 66
[4] Verboncoeur J P, Langdon A B and Gladd N T 1995 *Comput. Phys. Commun.* **87** 199
[5] Verboncoeur J P, Alves M V, Vahedi V and Birdsall C K 1993 *J. Comput. Phys.* **104** 321
[6] Gudmundsson J T and Lieberman M A 1998 *Plasma Sources Sci. Technol.* **7** 1
[7] Gudmundsson J T, Kouznetsov I G, Patel K K and Lieberman M A 2001 *J. Phys. D: Appl. Phys.* **34** 1100
[8] Gudmundsson J T 2004 *J. Phys. D: Appl. Phys.* **37** 2073
[9] Kim S, Lieberman M A, Lichtenberg A J and Gudmundsson J T 2006 *J. Vac. Sci. Technol.* A **24** 2025
[10] Gudmundsson J T and Thorsteinsson E G 2007 *Plasma Sources Sci. Technol.* **16** 399
[11] Vahedi V and Surendra M 1995 *Comput. Phys. Commun.* **87** 179
[12] Lichtenberg A J, Vahedi V, Lieberman M A and Rognlien T 1994 *J. Appl. Phys.* **75** 2339
[13] Lee S H, Iza F and Lee J K 2006 *Phys. Plasmas* **13** 057102
[14] Babaeva N Y, Lee J K, Shon J W and Hudson E A 2005 *J. Vac. Sci. Technol.* A **23** 699
[15] Roberto M, Verboncoeur J, Verdonck P and Cizzoto E 2006 *ECS Trans.* **4** 563
[16] Bronold F X, Matyash K, Tskhakaya D Schneider R and Fehske H 2007 *J. Phys. D: Appl. Phys.* **40** 6583
[17] Matyash K, Schneider R, Dittmann K, Meichsner J, Bronold F X and Tskhakaya D 2007 *J. Phys. D: Appl. Phys.* **40** 6601
[18] Schüngel E, Zhang Q-Z, Iwashita S, Schulze J, Hou L-J Wang Y-N and Czarnetzki U 2011 *J. Phys. D: Appl. Phys.* **44** 285205
[19] Bera K, Rauf S and Collins K 2011 *AIP Conf. Proc.* **1333** 1027
[20] Bera K, Rauf S and Collins K 2011 *IEEE Trans. Plasma Sci.* **39** 2576
[21] Itikawa Y 2009 *J. Phys. Chem. Ref. Data* **38** 1
[22] Shyn T W and Sweeney C J 2000 *Phys. Rev.* A **62** 022711
[23] Green M A, Teubner P J O, Brunger M J Cartwright D C and Campbell L 2001 *J. Phys. B: At. Mol. Opt. Phys.* **34** L157
[24] Lawton S A and Phelps A V 1978 *J. Chem. Phys.* **69** 1055
[25] Phelps A V 1985 *Technical Report* JILA Information Center Report 28, University of Colorado at Boulder http://jilawww.colorado.edu/~avp/collision_data/electronneutral/electron.txt
[26] Krishnakumar E and Srivastava S K 1992 *Int. J. Mass Spectrom. Ion Process* **113** 1
[27] Rapp D and Briglia D 1965 *J. Chem. Phys.* **43** 1480
[28] Locht R and Schopman J 1974 *Int. J. Mass Spectrom. Ion Phys.* **15** 361
[29] Thomas L D and Nesbet R K 1975 *Phys. Rev.* A **12** 1729
[30] Itikawa Y and Ichimura A 1990 *J. Phys. Chem. Ref. Data* **19** 637
[31] Laher R R and Gilmore F R 1990 *J. Phys. Chem. Ref. Data* **19** 277
[32] Kim Y-K and Desclaux J-P 2002 *Phys. Rev.* A **66** 012708
[33] Mul P M and McGowan J W 1979 *J. Phys. B: At. Mol. Phys.* **12** 1591
[34] Peverall R *et al* 2001 *J. Chem. Phys.* **114** 6679
[35] Guberman S L 1988 *Planet. Space Sci.* **36** 47
[36] Padgett R and Peart B 1998 *J. Phys. B: At. Mol. Opt. Phys.* **31** L995
[37] Olson R E 1972 *J. Chem. Phys.* **56** 2979
[38] Hayton D A and Peart B 1993 *J. Phys. B: At. Mol. Opt. Phys.* **26** 2879
[39] Vejby-Christensen L, Kella D, Mathur D, Pedersen H B, Schmidt H T and Andersen L H 1996 *Phys. Rev.* A **53** 2371
[40] Comer J and Schulz G J 1974 *J. Phys. B: At. Mol. Phys.* **7** L249
[41] Belostotsky S G, Economou D J, Lopaev D V and Rakhimova T V 2005 *Plasma Sources Sci. Technol.* **14** 532
[42] Ellis H W, Pai R Y, McDaniel E W, Mason E A and Viehland L A 1976 *At. Data Nucl. Data Tables* **17** 177
[43] Baer T, Murray P T and Squires L 1978 *J. Chem. Phys.* **68** 4901
[44] Wilcox J B and Moran T F 1981 *J. Phys. Chem.* **85** 989
[45] Brunetti B, Liuti G, Luzzatti E, Pirani F and Vecchiocattivi F 1981 *J. Chem. Phys.* **74** 6734
[46] Lindsay B G and Stebbings R F 2005 *J. Geophys. Res.* **110** A12213

[47] Stebbings R F, Smith A C H and Ehrhard H 1964 *J. Geophys. Res.* **69** 2349
[48] Stebbings R F, Smith A C H and Gilbody H B 1963 *J. Chem. Phys.* **38** 2280
[49] Muschlitz E E 1959 *Proc. IV Int. Conf. on Phenomena in Ionized Gases* (*Uppsala, Sweden, 17–21 August 1959*) ed N R Nilsson (Amsterdam: North-Holland) pp 52–6
[50] Lieberman M A and Lichtenberg A J 2005 *Principles of Plasma Discharges and Materials Processing* 2nd edn (New York: Wiley)
[51] Stebbings R F 1966 *Advances in Chemical Physics: Molecular Beams* vol 10 ed J Ross (New York: Wiley) pp 195–246
[52] Kawamura E, Birdsall C K and V Vahedi 2000 *Plasma Sources Sci. Technol.* **9** 413
[53] Nguyen C 2006 *Master's Thesis* University of California at Berkeley
[54] Lim C-H 2007 *PhD Thesis* University of California at Berkeley
[55] Miller R H and Combi M R 1994 *Geophys. Res. Lett.* **21** 1735
[56] Bruhwiler D L, Giacone R E, Cary J R, Verboncoeur J P, Mardahl P, Esarey E, Leemans W P and Shadwick B A 2001 *Phys. Rev. ST—Accel. Beams* **4** 101302
[57] Surendra M, Graves D B and Jellum G M 1990 *Phys. Rev.* A **41** 1112
[58] Okhrimovskyy A, Bogaerts A and Gijbels R 2002 *Phys. Rev.* E **65** 037402
[59] Bethe H A 1953 *Phys. Rev.* **89** 1256
[60] Fernández-Varea J M, Mayo R, Baró J and Salvat F 1993 *Nucl. Instrum. Methods Phys. Res.* B **73** 447
[61] Birdsall C K and Langdon B A 1991 *Plasma Physics Via Computer Simulation* (Bristol: Institute of Physics Publishing) Appendix C
[62] Thorsteinsson E G and Gudmundsson J T 2010 *Plasma Sources Sci. Technol.* **19** 055008